A Rigid Multibody Model to Study the Translational Motion of Guidewires Based on Their Mechanical Properties

Sharei Amarghan, Hoda; Kieft, Jeroen; Takashima , Kazuto ; Hayashida, Norihiro ; van den Dobbelsteen, John; Dankelman, Jenny

DOI
10.1115/1.4043618

Publication date
2019

Document Version
Final published version

Published in
Journal of Computational and Nonlinear Dynamics

Hoda Sharei
Faculty of Mechanical, Maritime and Materials Engineering,
Department of Biomechanical Engineering,
Delft University of Technology,
Mekelweg 2,
Delft 2628 CD, The Netherlands
e-mail: hoda.sharei@gmail.com

Jeroen Kieft
Faculty of Mechanical, Maritime and Materials Engineering,
Department of Biomechanical Engineering,
Delft University of Technology,
Mekelweg 2,
Delft 2628 CD, The Netherlands

Kazuto Takashima
School of Life Science and Systems Engineering,
Kyushu Institute of Technology,
2-4 Hibikino,
Wakamatsu-ku,
Kitakyushu 808-0196, Japan

Norihiro Hayashida
School of Life Science and Systems Engineering,
Kyushu Institute of Technology,
2-4 Hibikino,
Wakamatsu-ku,
Kitakyushu 808-0196, Japan

John J. van den Dobbelsteen
Faculty of Mechanical, Maritime and Materials Engineering,
Department of Biomechanical Engineering,
Delft University of Technology,
Mekelweg 2,
Delft 2628 CD, The Netherlands

Jenny Dankelman
Faculty of Mechanical, Maritime and Materials Engineering,
Department of Biomechanical Engineering,
Delft University of Technology,
Mekelweg 2,
Delft 2628 CD, The Netherlands

A Rigid Multibody Model to Study the Translational Motion of Guidewires Based on Their Mechanical Properties

During percutaneous coronary interventions (PCI), a guidewire is used as an initial way of accessing a specific vasculature. There are varieties of guidewires on the market and choosing an appropriate one for each case is critical for a safe and successful intervention. The main objective of this study is to predict the behavior of the guidewire and its performance in a vasculature prior to the procedure. Therefore, we evaluate the effectiveness of different mechanical properties of the guidewire on its behavior. A two-dimensional (2D) model has been developed in which a guidewire is considered as a set of small rigid segments connected to each other by revolute joints. These joints have two degrees-of-freedom to allow rotation. Linear torsional springs and dampers are applied in each joint to account for the elastic properties of the guidewire; the elastic properties have been measured for two commercially available guidewires (Hi-Torque Balance Middleweight Universal II—Abbot and Amplatz Super Stiff—Boston Scientific) and these are used in the model. Only translational motion has been applied to the guidewires and the effect of bending stiffness of the guidewire and also friction between guidewire and vasculature on its behavior are investigated. The results are validated with actual movement of the guidewires in a simple phantom model. Behavior of a guidewire in a vasculature was predicted using the developed model. The results of both simulation and experiment show that the behavior of a guidewire is influenced by its mechanical properties and by the friction between the guidewire and vasculature. This study is the first step to develop a complete model, which can predict the behavior of a guidewire inside the vasculature. We compared the tip trajectory for two commercial guidewires in one vasculature geometry. In future, this kind of knowledge might support not only the interventionist in choosing the best suitable guidewire for a procedure but also the designer to optimize new instrument to have the desired behavior. [DOI: 10.1115/1.4043618]

Introduction

Over the past decade, more than 7.4 million people have died as a result of coronary artery disease, which is the narrowing or blockage of coronary arteries [1]. Percutaneous coronary intervention (PCI) is a minimally invasive procedure for diagnosis and treatment of coronary artery disease [2]. During PCI, initially, a guidewire is used to access a specific vasculature. The choice of guidewire plays an important role in the success of an intervention. Although there are different types of guidewires, a systematic classification of the characteristics of guidewires has not yet been defined and there is no metric to select an appropriate guidewire for a specific vasculature. Hence, interventionists tend to perform the procedure on the basis of their experience. The main objective of this study is therefore to predict the behavior of the guidewire in a vasculature and its performance prior to the procedure. To achieve this, we have developed a computationally efficient computer-based model and have endeavored to investigate a relation between different mechanical properties, focusing on the stiffness of the guidewire and friction, and its behavior. We start this paper by reviewing the essential preliminaries of components and performance characteristics of guidewires. Moreover, the geometrical properties of the selected vasculature are presented. Then, the developed model, a short introduction on the rigid multibody dynamics technique, the simulation environment and experimental setup are explained. Finally, we discuss the results on the basis of the properties of two commercial guidewires and evaluate the accuracy of the model by a validation experiment.

[1]Corresponding author.
Contributed by the Design Engineering Division of ASME for publication in the Journal of Computational and Nonlinear Dynamics. Manuscript received November 13, 2018; final manuscript received April 18, 2019; published online September 12, 2019. Assoc. Editor: Elena G. Tolkacheva.

Method

Preliminaries

Guidewire. A guidewire is a long, thin, and flexible wire commonly used in combination with a catheter to facilitate the navigation through the vasculature's branches. Each guidewire consists of three main components: *core*, *distal tip*, and *covering*. The core (or central part) of the guidewire is commonly made of stainless steel, nitinol, or combination of them. The material, diameter, and tapering of the core influence the performance of the guidewire. The distal tip, which is situated inside the vasculature during the procedure, has either a one piece (core-to-tip) or a two-piece (shaping ribbon) tip design and its length and diameter are influential in specifying the function of the guidewire. The covering varies along the length of the guidewire; at the distal tip, coils or a polymer are mostly used to provide more flexibility. Moreover, the distal part often has either a hydrophilic or hydrophobic coating to reduce the friction between the guidewire and the vasculature, and between the guidewire and the interventional devices over the guidewire (e.g., catheter or stent).

The wide range of guidewires available in the market is the result of a change in these components. In other words, the construction of a guidewire and its performance are inextricably interwoven and the smallest variation in each of the components changes the overall properties of the guidewire and its performance [3–12].

To describe the performance of a guidewire, several terms are used in literature such as pushability, trackability, bending stiffness/flexibility, and torqueability [5,11–17]. Based on these characteristics, one classification for guidewires is presented as: starting (e.g., balance middleweight), selective (e.g., Universal II, Glidwire), and exchange guidewires (e.g., Amplatz Super Stiff). This classification is mainly based on the requirements during different phase of a procedure [11] and although it gives a general grouping, the choice of a guidewire within each group is still subjective. We will focus on the influence of the flexibility/stiffness of the guidewire on its translational motion. Flexibility/stiffness is the resistance of a guidewire against bending deformation (also known as bending stiffness, bending rigidity, and flexural rigidity). To measure this property, the guidewire must be intact and unused, since cutting the guidewire into segments would have disrupted the structural integrity of the wire and produced inaccurate results. We have measured the bending stiffness of two guidewires with a three-point bending test method at different places along the length of new guidewires. In this method, the guidewire is set between two supports (Fig. 1). A semicircular loading nose, placed at a point midway between the supports, is displaced at a test speed of 1 mm/s. To limit the influence of the gravity, the force is applied horizontally. By means of an attached 10 N load cell (Kyowa Electronic Instruments Co., Ltd.), the reaction force experienced by the loading nose is continuously measured. For consistency in the results, the measurements were done in the middle of every 30 mm, for a length of 150 mm from the distal side (in total five points). The test was performed three times for each segment and the average and the standard deviation of the results are presented. Finally, *EI* is a measure for the bending stiffness and is calculated by [18]

$$EI = \frac{Fl^3}{48d}\left(\mathrm{N}\cdot\mathrm{m}^2\right) \tag{1}$$

in which F is the applied force, l is the length of the guidewire, and d is the maximum displacement of the segment. As EI consists of two terms: E is the Young's Modulus, and I is the cross-sectional inertia. Therefore, material and diameter of the core of the guidewire influence the bending stiffness.

Vasculature. During interventional procedures, it is not only the properties of the guidewire but also the properties of the vasculature that influence the choice of guidewire. Depending on the properties of a vasculature such as its diameter, angle in bifurcation, and stiffness of the wall, a different guidewire has to be chosen. Recent research on extracting the geometry of the vasculatures has yielded some interesting results [19–22], which inspired us with our phantom model (Fig. 2). Our vasculature model includes branches with diameters between 2 mm and 8 mm, and bifurcation angels between 60 deg and 120 deg. The ProJet 3500 HD three-dimensional (3D) printer is used to print the phantom model. Data regarding wall stiffness is extracted from the catalog of the printer (material: VisiJet M3 Crystal, flexural strength: 49 MPa) [23]. The guidewire cannot deform the vasculature phantom due to high stiffness of the material. Although we can take into account the deformation of the vascular wall in the simulation model, due to high value of the wall stiffness in the phantom model, deformation will be neglected.

Model. Modeling guidewires and catheters and their behavior within the vasculature, for different purposes, is an emerging research area and a variety of techniques have been used [3,22,24–36]. We have developed a multibody dynamic model to

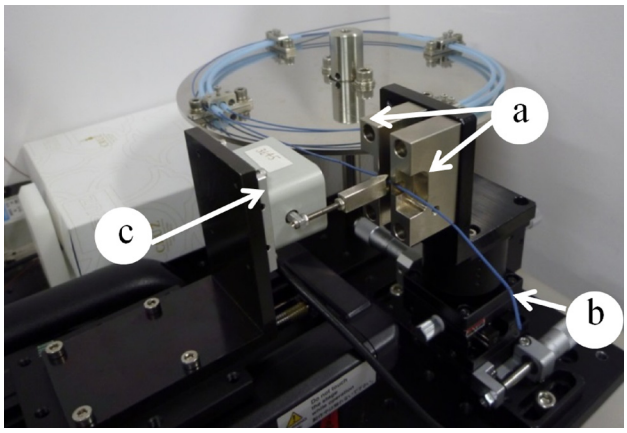

Fig. 1 Experimental setup: three-point bending test: (*a*) supports, (*b*) guidewire, and (*c*) load cell

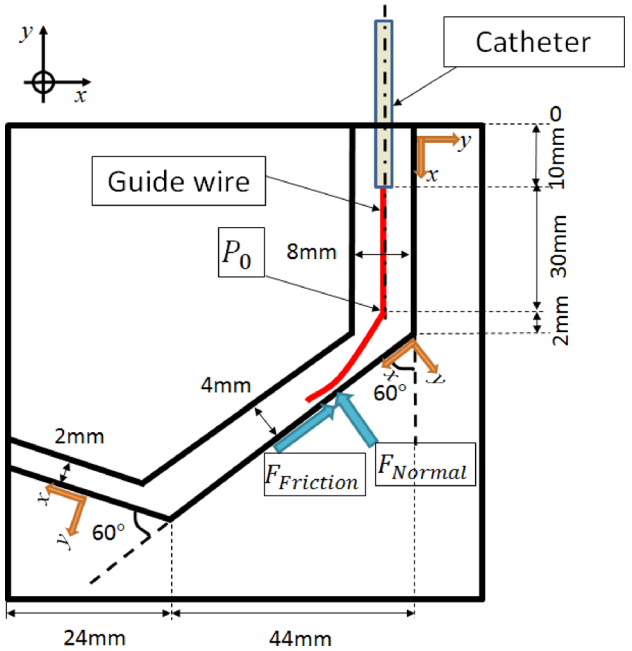

Fig. 2 Schematic of guidewire and vasculature interaction forces: P_0 is the initial position of the guidewire tip

simulate the translational motion of a guidewire. An advantage of this method is that because of its simple structure, it is easy to understand and in comparison with finite element method modeling, it is very fast. Moreover, adding other phenomena such as friction and/or material properties to different parts of the body is easier to incorporate [37]. In the following, we will first discuss the applied forces to the guidewire while navigating inside the vasculature. These forces play an important role in the orientation of the guidewire. Then, the multibody dynamics method will be explained to pave the way to formulate the equations of motion for the guidewire model.

Forces on the Guidewire Inside the Vasculature. Orientation of a guidewire inside the vasculature is determined by the applied forces (Fig. 2). Due to the contact with the vascular wall, collision and friction are considered as the most influential forces [38,39]. In case of a collision, detecting and responding to it are two important parts of the simulation. In our model, we have implemented a simple collision detection algorithm in which a collision occurs when the distance between the guidewire and the vasculature wall is smaller than the guidewire diameter. With x and y being the positions in x- and y-direction, we apply Eqs. (2) and (3) to add constraints to the contact force

$$|x| \leq \frac{1}{2} l_v \tag{2}$$

$$|y| \leq \frac{1}{2} t_v - r_{\text{wire}} \tag{3}$$

in which l_v and t_v are the length and the thickness of the vasculature, respectively, and r_{wire} is the radius of the guidewire. If the contact constraints are met, regarding the collision response, a normal force is exerted onto the wire. Since the vasculature is modeled as a spring-damper-system, the normal force consists of a spring component, calculated using the penetration depth (u) and a damping component calculated with the penetration velocity. This force prevents the guidewire from penetrating inside the vasculature wall and Hooke's law is used to account for it (the wall stiffness is based on material properties used in the phantom model)

$$u = \left(\frac{1}{2} t_v - r_{\text{wire}} - |y| \right) \tag{4}$$

$$F_n = -k_w \cdot u - c_w \cdot v_y \tag{5}$$

in which k_w and c_w are the spring stiffness and the damping coefficient and v_y is the speed of guidewire in y-direction. For the friction between the guidewire and the vasculature wall, the Coulomb friction model is used; the friction force is calculated from the normal force (F_n) by multiplying it with a friction coefficient (μ)

$$F_f = F_n \cdot \mu \cdot \left(-\frac{v_x}{|v_x|} \right) \tag{6}$$

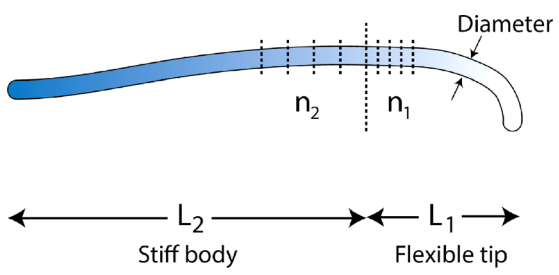

Fig. 3 Visual representation of guidewire model: the guidewire is considered as a chain of small rigid segments connected to each other by joints

in which v_x is the speed of guidewire in x-direction. When $|v_x| = 0$ (namely, static condition), F_f is zero. Therefore, only dynamic friction is considered in this equation. The value for the friction coefficient is based on information provided in Ref. [40].

Multibody Dynamics Model. The multibody dynamics approach follows a discrete representation of a continuum body. The body is discretized to smaller segments interconnected with each other by joints [41–43]. The dynamic behavior of the total system is investigated by deriving and solving the equations of motion of the whole body [26,27,44–46]. The segments are considered as rigid bodies, i.e., each segment can translate and rotate but its shape is fixed.

Based on the above-explained theory of multibody dynamics, we consider the guidewire as a set of rigid segments. As the guidewire is under planar motion, revolute joints are used between each two segments to allow for rotation. The length of the segments is variable: the segments at the distal end have shorter length than at the proximal end (Fig. 3). This is due to the variation in mechanical properties of the guidewire along the length: more flexible at the distal side and more stiff at the proximal side. In the modeling, the proximal side of the guidewire is inserted into a catheter, which is fixed and is considered as the initial position of the guidewire, and the distal side of guidewire, which is outside the catheter, navigates inside the vasculature.

Mathematical Formulation of Equations of Motion. The developed model is based on the forward dynamic method, i.e., given initial conditions and applied forces and/or applied moments, over a given time interval to predict the motion. By applying a defined force to the proximal side of the guidewire, the tip moves by a speed of 2 mm/s. We defined the relative position of each two segments by means of the relative angle between them (θ_i). Thus, the motion is described by the generalized coordinates $[\theta_1, \theta_2, \ldots, \theta_n]$ and the coordinates of each joint α_i are expressed as

$$\alpha_i = T_i(\theta_i) \tag{7}$$

in which T_i is the transformation matrix. The corresponding velocity and acceleration of joint α_i in the new coordinate system are then

$$\dot{\alpha}_i = \frac{\partial T_i}{\partial \theta_i} \dot{\theta}_i \tag{8}$$

$$\ddot{\alpha}_i = \frac{\partial T_i}{\partial \theta_i} \ddot{\theta}_i + \frac{\partial^2 T_i}{\partial \theta_i \partial \theta_j} \dot{\theta}_i \dot{\theta}_j \tag{9}$$

To account for the bending stiffness of the guidewire, linear torsional springs and dampers are applied in the joints. From the mechanics of materials [18], the relation between the torque T_s and the angle of twist in a torsional spring is

$$T_s = k(\theta - \theta_0) \tag{10}$$

where k is the torsional spring stiffness, θ_0 is the neutral angle where restoring torque is zero, and θ is the joint angle. In the same way, for the torsional viscous damper, we have

$$T_d = C\dot{\theta} \tag{11}$$

in which C is the torsional coefficient of viscous damping and $\dot{\theta}$ is the joint angular velocity. From Ref. [18] and based on Eqs. (10) and (11), the differential equation of motion for a n-degrees-of freedom system is written in the matrix form as

$$M\ddot{\alpha} + D\dot{\alpha} + K(\alpha - \alpha_0) = Q \tag{12}$$

where M is the mass matrix, D and K are damping and stiffness matrices, α_0 is the angular position in equilibrium, and Q is the

vector of generalized nonconservative forces. As the mass of each segment of the guidewire is very small compared to its length, it can be neglected (i.e., $M \approx 0$). Substituting Eqs. (8) and (9) into Eq. (12), and conducting a number of simplifications, we have

$$-D\dot{\theta} = -T^{\mathrm{T}}(F + M_t) + K(\theta - \theta_0) \tag{13}$$

where T is the transformation matrix that transfers the global coordinates to local coordinates, F and M_t contain the applied forces and the applied moments, respectively. The derived equation (Eq. (13)) consists of a set of equations where all of them are needed to be solved at the same time (simultaneous or coupled equations [26]).

Simulation. We simulated the translational motion of the guidewire inside the vasculature and assessed the effect of different parameters: bending stiffness of the guidewire, friction between guidewire and vasculature wall, and the transition of applied force on the guidewire. Moreover, as we discretized the guidewire to smaller segments, the influence of number of segments (n) on the computation time and the accuracy of simulation is investigated. The measured data of Hi-Torque Balance Middleweight Universal II-Abbot and Amplatz Super Stiff—Boston Scientific guidewires (Fig. 4) are used regarding the bending stiffness. We will refer to these two guidewires as Universal and Amplatz. The model is developed in a MATLAB/SIMULINK (The MathWorks, Inc.) environment. In Table 1 and Fig. 4, the guidewires' parameters used in the simulation are listed (see Fig. 3).

Experiment. The experimental setup for the validation is shown in Fig. 5. Details about the setup are explained in Ref. [43]. We inserted the two guidewires, which were also used in the simulation (Universal and Amplatz), into the phantom model using a two-axis automatic stage (Sigma Koki Co., Ltd., SGSP20-85(X), SGSP-40YAW). The guidewire is manipulated by pushing and pulling at the proximal side. One camera (15 frames per second, 1920×1080 screen resolution (Logicool)), positioned in front of the model, is used to record the trajectory during the experiment. Furthermore, 10 N load cells are placed under the phantom model to measure the applied forces in y-direction. Since the applied forces for Universal guidewire were very small, we have changed the load cells to 1 N to be able to measure small forces. Finally, to evaluate the accuracy of the simulation, the trajectory results are compared and the root-mean-square is calculated to measure error as follows:

$$\text{error} = \sqrt{\frac{1}{i}\sum_i \sum_j \left(P^V_{\text{tip}}(i) - P^S_{\text{tip}}(j)\right)^2} \tag{14}$$

in which P^V_{tip} and P^S_{tip} are the position of the distal tip in the experiment and in the simulation, respectively.

Results

Bending Stiffness. Figure 4 shows the results of bending stiffness measurement for the two guidewires: Amplatz and Universal. It can be seen that, although the bending stiffness is nonhomogeneous along the length of the guidewire(s), it follows almost the same pattern for both guidewires: first a considerable flexibility at the distal side, then an abrupt increase in the transition part toward the proximal side. In Fig. 6, the propagation of the two guidewires with different bending stiffness is shown. These results show that the flexibility of a guidewire impacts its behavior during advancement: a higher flexibility results in a different trajectory and more contact with the vasculature wall.

Number of Segments and Error Measurement. The total number of segments (n) to define the length of the guidewire in the simulation model has a significant effect on the behavior and the computation time. Figure 7 shows that lower number of segments results into bigger error. On the other hand, increasing the number above a certain threshold does not change the behavior anymore, but the computation time increases (Table 2). Moreover, comparing the results for two guidewires shows that the stiffer guidewire (Amplatz) is more sensitive to the number of segments.

Friction Coefficient and Applied Forces. Figure 8 shows the transition of applied force between the guidewire and vasculature wall along the y-axis for both Amplatz and Universal guidewires in the experiments. These results show that the contact force is much higher for the stiffer guidewire. Furthermore, the contact force is influenced by the geometry of vasculature, i.e., there are peaks in the applied force in the corners. At $t = 22$ s in Fig. 9, a small peak is seen, which is due to the contact with the wall in the second corner. In Fig. 9, the effect of friction for Amplatz guidewire is assessed and is shown that with a higher friction coefficient the contact force increases.

Discussion and Conclusion

The goal of this study was to develop a guidewire simulation model and predict the behavior of the guidewire and its performance inside a vasculature. We have investigated the effect of

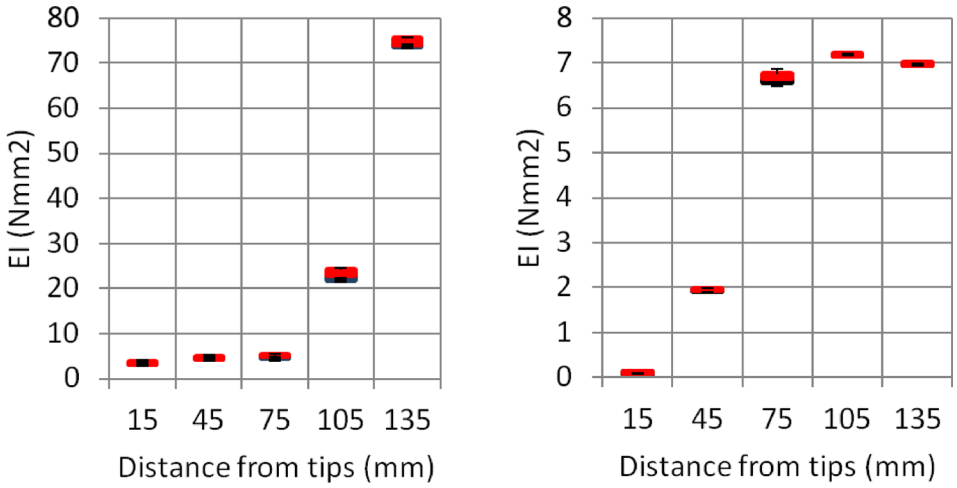

Fig. 4 Bending stiffness measurement: (*a*) Amplatz and (*b*) Universal

Table 1 Guidewires data

Name and trade	Diameter (mm)	Core material	Flexible tip (mm)	Length used in simulation (mm)
Amplatz Super Stiff (Boston Scientific)	0.89	Stainless steal	70	150
Universal II (Abbot Vascular)	0.36	Nitinol	45	150

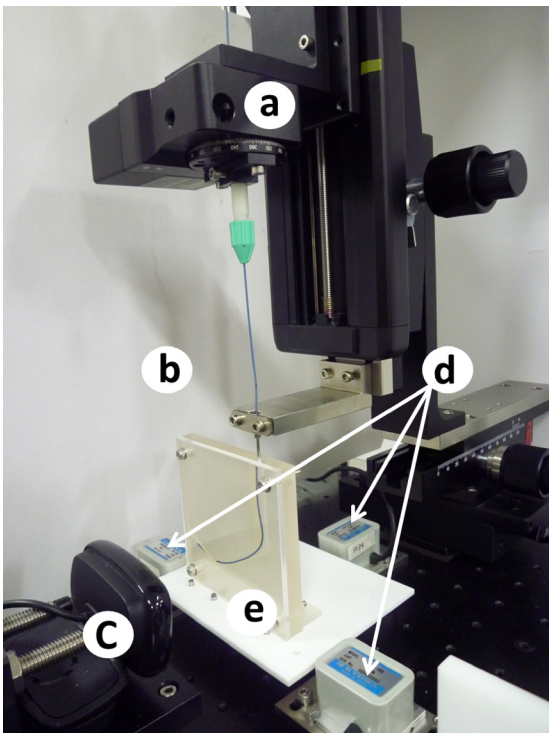

Fig. 5 Experimental setup: (*a*) automatic stage, (*b*) guidewire, (*c*) camera, (*d*) load cell, and (*e*) phantom model

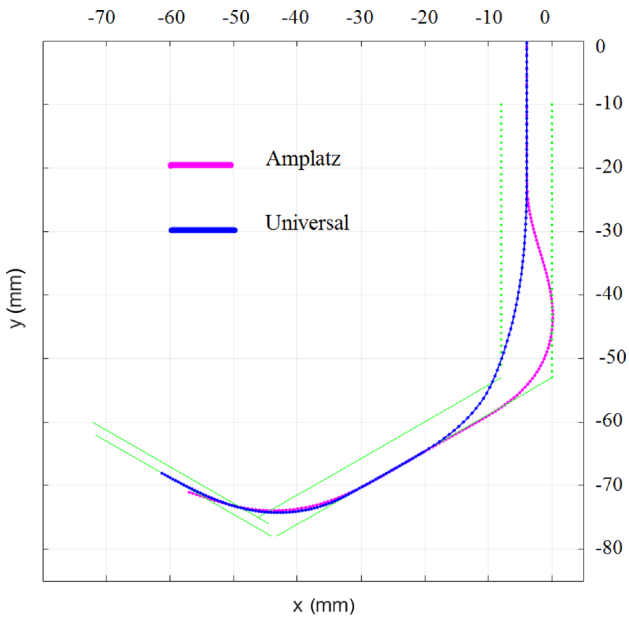

Fig. 6 Comparing the trajectory of Amplatz and Universal guidewires in simulation for $n = 200$

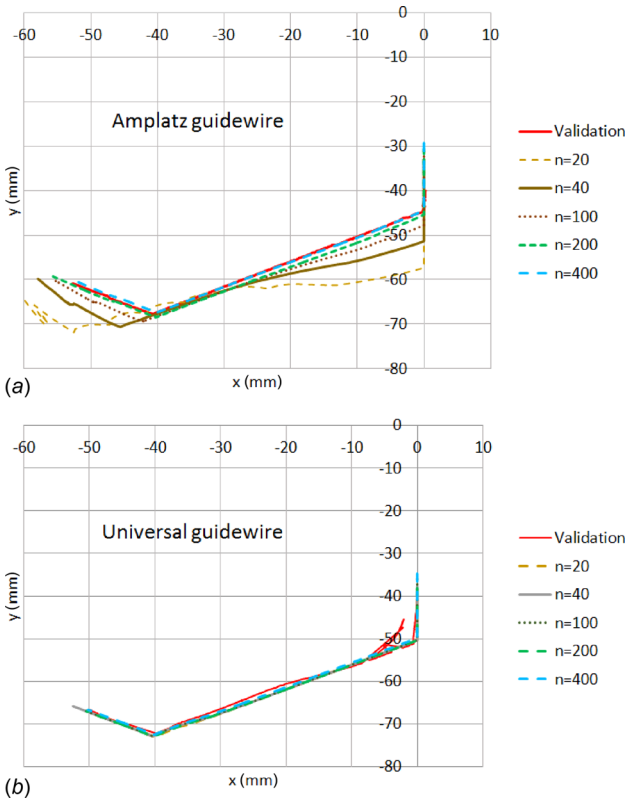

Fig. 7 Trajectory of the tip of the guidewires in the simulation and the validation experiment: (*a*) Amplatz and (*b*) Universal

bending stiffness and friction on the behavior of a guidewire and validated the results.

Bending Stiffness. The results of bending stiffness measurement conform with the expected properties from a guidewire: sufficient flexibility at the tip to pass through the vasculatures and high rigidity in the body to transfer the force from the proximal side. Moreover, the results confirm that the guidewire with nitinol has more flexibility than the one with stainless steel. The developed model has shown how these differences influence the behavior of the guidewire inside the vasculature: e.g., a guidewire with higher flexibility results in less contact force with the vasculature wall. This can be explained by the fact that the flexible tip deflects easier than the stiff one and thus, it needs less force to navigate. This property also affects the simulation time; in the simulation, the flexible one takes slightly longer than the stiff one to be computed (Table 2).

Table 2 Simulation computation time for different number of segments and error measurement, friction coefficient = 0.4

Guidewire	Number of segments	Computation time (s)	Error (mm)
Universal II—Abbot Vascular	20	4	4.91
	40	15	3.12
	100	96	1.68
	200	469	0.87
	400	3534	0.38
Amplatz Super Stiff—Boston Scientific	20	4	0.76
	40	14	0.70
	100	91	0.69
	200	455	0.56
	400	2857	0.56

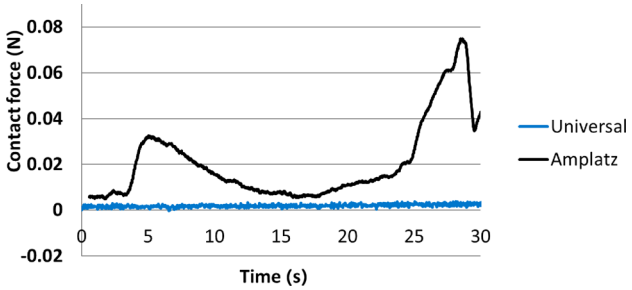

Fig. 8 Comparing the transition of applied forces for two guidewires: Amplatz and Universal

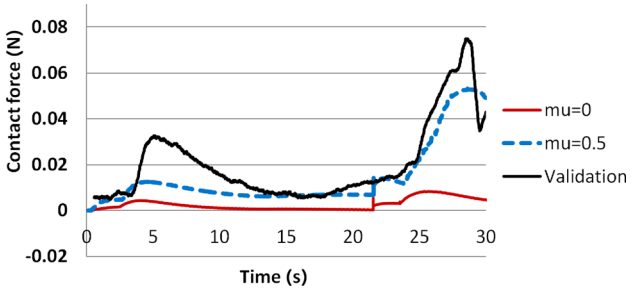

Fig. 9 Comparing the transition of applied forces between guidewire and vasculature wall along *y*-axis in simulation ($n = 200$) with different friction coefficient and the validation experiment: Amplatz guidewire

Friction. We have changed the friction coefficient in the simulation to see the effect of this parameter on the behavior. It has been shown that more friction causes the guidewire to navigate with more bending and the tip applies more force to the vasculature wall.

Limitation. 3D printed model has been used for the experiments. The material of this model has a flexural strength of 49 MPa, which is very stiff relative to a guidewire, i.e., a guidewire cannot deform the vasculature. In the simulation, although it is possible to consider the deformation of the vascular wall, due to high value of the wall stiffness in the phantom model, deformation was neglected.

The differences between simulation and experiments may be due to the following reasons:

- Only the translational motion in two-dimensional has been investigated. Thus, a perfect torque control is assumed.
- Estimated data regarding friction and high stiffness for vasculature wall are used.
- Plastic deformation of the guidewire during the experiments is ignored.

This study is the first step to develop a complete model which can predict the behavior of a guidewire inside the vasculature. We have investigated the trajectory of two guidewires with different mechanical properties. We conclude that knowledge of the behavior of the guidewire might help the interventionist to choose an appropriate one. Furthermore, this information makes the design requirements clear and might help to optimize new instruments to follow the desired behavior.

For future research, we will extend the model to 3D with a deformable wall and the combination of a guidewire and a catheter will be modeled. The main challenge to extend the two-dimensional model to 3D model is having more degrees-of-freedom in each joint to model the full motion of the instrument; therefore, we need different type of joints in the guidewire model in order to be able to model three translations and three rotations. Moreover, we will modify the simulation parameters to minimize the differences of the guidewire behavior in the experimental and simulation results.

Acknowledgment

The authors would like to thank Dr. Kiyoshi Yoshinaka (National Institute of Advanced Industrial Science and Technology, Japan) for supporting us with the image processing software.

H. S. performed the main modeling and analyzed the results. J. K. made substantial contributions to the modeling. N. H. and K. T. established the validation experiments. J. J. D. and J. D. contributed to the data interpretation and discussion of the research findings. J. D. acquired the funding for this research and she made critical revisions to the manuscript.

Funding Data

- This work is part of the research program CONNECT project (Grant No. 12705) within the research program interactive Multi-Interventional Tools (iMIT), which is supported by the Dutch Technology Foundation STW, which is part of The Netherlands Organization for Scientific Research (NWO) (Funder ID: 10.13039/501100003246).

Nomenclature

Symbol Description

C = torsional coefficient of viscous damping
d = maximum displacement
D = damping matrix
E = Young's modulus
F = applied force
F_D = received force at the distal side
F_P = applied force at the proximal side
I = cross-sectional inertia
k = torsional spring stiffness
K = stiffness matrix
k_w = vasculature wall stiffness
K_t = rotational stiffness
L = guidewire length
m = number of force measurements
M = mass matrix
M_t = applied moment
n = number of segments
Q = generalized nonconservative forces
t = wall thickness
T = transformation matrix that transfers the global coordinates to local coordinates
T_d = torsional viscous damper
T_s = torque
α_i = coordinates of joint i
α_0 = angular position in equilibrium
θ = rotation angle
$\dot{\theta}$ = joint angular velocity
θ_0 = neutral angle where restoring torque is zero
$\dot{\theta}_0$ = joint angular velocity where T_d is zero
λ_i = segment length

References

[1] WHO, 2015, "lThe Top 10 Causes of Death," World Health Organization, Geneva, Switzerland, Accessed Apr. 15, 2015, http://www.who.int/media-centre/factsheets/fs310/en/

[2] Smith, S. C., Jr. Dove, J. T., Jacobs, A. K., Kennedy, J. W., Kereiakes, D., Kern, M. J., Kuntz, R. E., Popma, J. J., Schaff, H. V., and Williams, D. O., 2001, "ACC/AHA Guidelines of Percutaneous Coronary Interventions (Revision of the 1993 PTCA Guidelines) Executive Summary," J. Am. Coll. Cardiol., **37**(8), pp. 2215–2239.

[3] El-Khalili, N. H., 1999, "Surgical Training on the World Wide Web," Ph.D. dissertation, The University of Leeds, Leeds, UK.

[4] Lanzer, P., ed., 2012, *Catheter-Based Cardiovascular Interventions: A Knowledge-Based Approach*, Springer Science and Business Media, London, pp. 469–471.
[5] Erglis, I., Narbute, D., Sondore, A., Grave, S., and Jegere, 2010, "Tools and Techniques: Coronary Guidewires," EuroIntervention, **6**, 1–8.
[6] Tóth, G.G., Yamane, M., and Heyndrickx, G. R., 2014, "How to Select a Guidewire: Technical Features and Key Characteristics," Heart, **101**(8), pp. 645–652.
[7] Craig, W., 2013, "Guidewire Selection for Peripheral Vascular Interventions," Endovascular Today, **5**, pp. 80–83.
[8] Colombo, A., Babic, R., and Corbett, S., 2007, "Coronary Guidewires," *Problem Oriented Approaches in Interventional Cardiology*, CRC press, Boca Raton, FL, Chap. 2.
[9] Ramanath, V. S., and Thompson, C. A., 2014, "Guidewires and Angioplasty Balloons: The Primer," *Textbook of Cardiovascular Intervention*, Springer, London, pp. 91–98.
[10] Ellis, S. G., and Holmes, D. R., 2005, *Strategic Approaches in Coronary Intervention*, 3rd ed., Philadelphia, PA, pp. 91–100.
[11] Schneider, P. A., 2008, *Endovascular Skills: Guidewire and Catheter Skills for Endovascular Surgery*, 3rd ed., CRC press, Boca Raton, FL.
[12] von Schmilowski, E., and Swanton, R. H., 2012, *Essential Angioplasty*, Wiley, Hoboken, NJ, Chap. 2.
[13] Topaz, O., ed., 2015, *Lasers in Cardiovascular Interventions*, Springer, London, pp. 8–9.
[14] Schmidt, W., Lanzer, P., Behrens, P., Topoleski, L. D., and Schmitz, K. A., 2009, "Comparison of the Mechanical Performance Characteristics of Seven Drug-Eluting Stent Systems," Catheter Cardiovasc. Interventions, **73**(3), pp. 350–360.
[15] Wunderlich, C. B., Schmidt, W., Behrens, P., Schmitz, K.-P., 2012, "The Effect of Different Guide Wires on the Trackability of Coronary Stent Delivery Systems," Biomed. Eng., **57**(SI-1), p. 880881.
[16] Mishra, S., and Bahl, V. K., 2009, "Curriculum in Cath Lab: Coronary Hardware—Part II: Guidewire Selection for Coronary Angioplasty," Indian Heart J., **61**(1), pp. 178–185.
[17] Sutou, Y., Yamauchi, K., Suzuki, M., Furukawa, A., Omori, T., Takagi, T., Kainuma, R., Nishida, M., and Ishida, K., 2006, "High Maneuverability Guidewire With Functionally Graded Properties Using New Superelastic Alloys," Minimally Invasive Ther. Allied Technol., **15**(4), pp. 204–208.
[18] Meirovitch, L., 2000, *Fundamentals of Vibrations*, Waveland Press, Long Grove, IL, pp. 23–39.
[19] Pflederer, T., Ludwig, J., Ropers, D., Daniel, W. G., and Achenbach, S., 2006, "Measurement of Coronary Artery Bifurcation Angles by Multidetector Computed Tomography," Invest. Radiol., **41**(11), pp. 793–798.
[20] Dodge, J. T., Jr, Brown, B. G., Bolson, E. L., and Dodge, H. T., 1992, "Lumen Diameter of Normal Human Coronary Arteries. Influence of Age, Sex, Anatomic Variation, and Left Ventricular Hypertrophy or Dilation," Circulation, **86**(1), pp. 232–246.
[21] Clogenson, H., 2014, "MRI-Compatible Endovascular Instruments: Improved Maneuverability During Navigation," Ph.D. thesis, Delft University, Delft, The Netherlands.
[22] Konings, M. K., van de Kraats, E. B., Alderliesten, T., and Niessen, W. J., 2003, "Analytical Guide Wire Motion Algorithm for Simulation of Endovascular Interventions," Med. Biol. Eng. Comput., **41**(6), pp. 689–700.
[23] 3D Systems, 2017, "Easily Create High-Definition, Precise Plastic Functional-Prototypes and End-Use Parts," Sydney, Australia, Accessed Jan. 25, 2017, http://ja.3dsystems.com/sites/www.3dsystems.com/files/projet_3500_plastic_0115_usen_web.pdf
[24] Guilloux, V., Haigron, P., Goksu, C., Kulik, C., and Lucas, A., 2006, "Simulation of Guidewire Navigation in Complex Vascular Structures," SPIE Paper No. 614107.
[25] Rosen, J. M., Soltanian, H., Redett, R. J., and Laub, D. R., 1996, "Evolution of Virtual Reality [Medicine]," IEEE Eng. Med. Biol. Mag., **15**(2), pp. 16–22.
[26] Ikuta, K., Iritani, K., Fukuyama, J., and Takeichi, M., 2000, "Portable Virtual Endoscope System With Force and Visual Display for Insertion Training," IEEE/RSJ International Conference on Intelligent Robots and Systems (IROS), Berlin, Germany, Oct. 11, p. 720726.
[27] Kukuk, M., 2002, "A Model-Based Approach to Intraoperative Guidance of Flexible Endoscopy," Ph.D. thesis, Dortmund University, Princeton, NJ.
[28] Seo, J.-H., Jung, I.-H., Park, T.-W., and Chai, J.-B., 2005, "Dynamic Analysis of a Multibody System Including a Very Flexible Beam Element," JSME Int. J., Ser. C, **48**(2), pp. 224–233.
[29] Alderliesten, T., 2004, "Simulation of Minimally-Invasive Vascular Interventions for Training Purposes," Ph.D. thesis, Utrecht University, Utrecht, The Netherlands.
[30] Tang, W., Wan, T. R., Gould, D. A., How, T., and John, N. W., 2012, "A Stable and Real-Time Nonlinear Elastic Approach to Simulating Guidewire and Catheter Insertions Based on Cosserat Rod," IEEE Trans. Biomed. Eng., **59**(8), pp. 2211–2218.
[31] Mi, S.-H., Hou, Z.-G., Yang, F., Xie, X.-L., and Bian, G.-B., 2013, "A Multi-Body Mass-Spring Model for Virtual Reality Training Simulators Based on a Robotic Guide Wire Operating System," IEEE International Conference on Robotics and Biomimetics (ROBIO), Shenzhen, China, Dec. 12–14, pp. 2031–2036.
[32] Wang, Y. P., Chui, C. K., Cai, Y. Y., and Mak, K. H., 1997, "Topology Supported Finite Element Method Analysis of Catheter Guidewire Navigation in Reconstructed Coronary Arteries," IEEE Comput. Cardiol., **24**, pp. 529–532.
[33] Wang, Y., Chui, C., Lim, H., Cai, Y., and Mak, K., 1998, "Real-Time Interactive Simulator for Percutaneous Coronary Revascularization Procedures," Comput. Aided Surg., **3**(5), p. 211.
[34] Li, Z., Chui, C.-K., Anderson, J. H., Chen, X., Ma, X., Hua, W., Peng, Q., Cai, Y., Wang, Y., and Nowinski, W. L., 2001, "Computer Environment for Interventional Neuroradiology Procedures Zirui," Simul. Gaming, **32**(3), pp. 404–419.
[35] Schafer, S., Singh, V., Noel, P. B., Walczak, A. M., Xu, J., and Hoffmann, K. R., 2009, "Real-Time Endovascular Guidewire Position Simulation Using Shortest Path Algorithms," Int. J. Comput. Assisted Radiol. Surg., **4**(6), pp. 597–608.
[36] Khatait, J., 2013, "Motion and Force Transmission of a Flexible Instrument Inside a Curved Endoscope," Ph.D. thesis, University of Twente, Enschede, The Netherlands.
[37] Burgner-Kahrs, J., Caleb Rucker, D., and Choset, H., 2015, "Continuum Robots for Medical Applications: A Survey," IEEE Trans. Rob., **31**(6), pp. 1261–1280.
[38] Korner, O., and Manner, R., 2003, "Implementation of a Haptic Interface for a Virtual Reality Simulator for Flexible Endoscopy," 11th Symposium on Haptic Interfaces for Virtual Environment and Teleoperator Systems (HAPTICS 2003), Loss Angeles, CA, Mar. 22, pp. 278–284.
[39] Wei, P., Feng, Z.-Q., Xie, X.-L., Bian, G.-B., and Hou, Z.-G., 2014, "FEM-Based Guide Wire Simulation and Interaction for a Minimally Invasive Vascular Surgery Training System," 11th World Congress on Intelligent Control and Automation (WCICA), Shenyang, China, June 29–July 4, pp. 964–969.
[40] Schröder, J., 1993, "The Mechanical Properties of Guidewires—Part III: Sliding Friction," Cardiovasc. Interventional Radiol., **16**(2), pp. 93–97.
[41] Valembois, R. E., Fisette, P., and Samin, J.-C., 1997, "Comparison of Various Techniques for Modelling Flexible Beams in Multibody Dynamics," Nonlinear Dyn., **12**(4), pp. 367–397.
[42] de Jalon, J. G., and Bayo, E., 1994, *Kinematic and Dynamic Simulation of Multibody Systems: The Real-Time Challenge*, Springer-Verlag, New-York, p. 440.
[43] Takashima, K., Tsuzuki, S., Ooike, A., Yoshinaka, K., Yu, K., Ohta, M., and Mori, K., 2014, "Numerical Analysis and Experimental Observation of Guidewire Motion in a Blood Vasculature Model," Med. Eng. Phys., **36**(12), pp. 1672–1683.
[44] Stewart, D. E., 2000, "Rigid-Body Dynamics With Friction and Impact," Soc. Ind. Appl. Math., **42**(1), p. 339.
[45] Amirouche, F., 2007, *Fundamentals of Multibody Dynamics: Theory and Applications*, Springer Science & Business Media, London.
[46] Fritzkowski, P., and Kaminski, H., 2011, "A Discrete Model of a Rope With Bending Stiffness or Viscous Damping," Acta Mech. Sin., **27**(1), pp. 108–113.